DE GRUYTER

Chemical Papers 69 (2) 316–324 (2015)
DOI: 10.1515/chempap-2015-0029

ORIGINAL PAPER

Promoting effect of group VI metals on Ni/MgO for catalytic growth of carbon nanotubes by ethylene chemical vapour deposition

Ahmed E. Awadallah*

Process Development Division, Egyptian Petroleum Research Institute, Nasr City, Cairo 11787, Egypt

Received 20 November 2013; Revised 21 May 2014; Accepted 21 May 2014

The incorporation of 1 mass % of group VI metals (chromium, molybdenum, and tungsten) into 4 mass % of Ni/MgO catalysts was evaluated for the synthesis of carbon nanotubes (CNTs) by the catalytic chemical vapour deposition of ethylene. All materials were characterised by XRD, surface area, TEM, SEM, Raman spectroscopy, and TGA-DTA. The resulting data demonstrated that the addition of group VI metals improved the surface area and metal dispersion, thereby achieving a remarkable enhancement in catalytic growth activity. Among the metals of group VI, Mo was found to be the most effective promoter for catalysing the CNTs' growth. From TEM observation, long CNTs with a higher degree of graphitization were obtained on the Ni–Mo/MgO catalyst. TGA and DTA analysis showed that the as-grown CNTs over both Ni–Mo and Ni–W/MgO catalysts exhibited higher thermal stability.

Keywords: carbon nanotubes, chemical vapour deposition, nickel, transition metals, ethylene

Introduction

Carbon nanotubes (CNTs) have attracted tremendous research interest since their discovery in 1991. Their unique electrical, thermal, and mechanical properties present opportunities for numerous applications, including optical and electronic nano-devices, electrodes for fuel cell and Li ion batteries, chemical and biological sensors, and catalysts supports (de Lucas et al., 2005; Toebes et al., 2004; Fujiwara et al., 2001; Tans et al., 1998; Fan et al., 1999; Andersen et al., 2013; Chen et al., 2003). The catalytic chemical vapour deposition (CCVD) method can be considered as a simple and economical technique for large-scale production of CNTs at low temperature and ambient pressure in comparison with the arc-discharge and laser-ablation methods (Chen et al., 2006).

Transition metals of group VIII (Fe, Co, and Ni) are commonly used as active centres in the CCVD method. These metals possess both an ability to form carbides and allow carbon to diffuse through and over the metals extremely rapidly (Sinnott et al., 1999). Furthermore, Fe, Co, and Ni have partially filled 3d orbitals which facilitate the dissociation of the hydrocarbon molecules through partially accepting electrons. This interaction along with the "back-donation" from the metal into the unoccupied orbital in the hydrocarbon molecule changes the electronic structure of the adsorbed molecule so that the dissociation of the molecule occurs (Dupuis, 2005).

Catalyst supports play an essential role in the catalytic growth activity of CNTs. The main role of the support is to improve the dispersion and decrease the aggregation of metal particles during the reaction. In addition, the support has a great influence on the morphology of the carbon formed. Several substrates such as SiO_2, Al_2O_3, MgO, TiO_2, ZrO_2, La_2O_3, CeO_2, SiO_2/Al_2O_3, and zeolites are used as catalyst supports in the CCVD method (Cassell et al., 1999; Ago et al., 2006; Tang et al., 2001; Ni et al., 2006; Chen et al., 2009; Jehng et al., 2008; Li et al., 2006; Ashok et al., 2007). MgO possesses the advantage over these sup-

*Corresponding author, e-mail: ahmedelsayed_epri@yahoo.com

ports of being easy to remove during the purification of the as-grown carbon nanotubes (Takenaka et al., 2003; Zheng et al., 2004).

Promoters can also play a significant role in the catalytic activity. The promoter changes the electronic structure of the catalyst, lowering the activation energy for dissociation. This behaviour reduces the growth temperature, hence enhancing overall performance (Lee et al., 2000; Harutyunyan et al., 2002). Metals such as molybdenum, platinum, ruthenium, and copper have been used as a catalyst promoter with the active metals (Lee et al., 2000; Yeoh et al., 2010; Awadallah et al., 2014; Chai et al., 2006). Ago et al. (2006) studied the Fe–Mo/MgO catalyst for the synthesis of single-wall carbon nanotubes (SWCNTs). They found that Mo suppresses the formation of excess amorphous carbon on the surface of Fe particles during the nanotubes' growth, thereby preventing the rapid deactivation of the catalyst. A synergetic effect between cobalt and molybdenum was also discovered by Tang et al. (2001). They found that the addition of molybdenum to the Co/MgO catalyst increased the yield and improved the quality of SWCNTs.

In comparison with molybdenum, few papers have reported the use of chromium and tungsten for the synthesis of carbon nanotubes (Loebick et al., 2009, 2010; Pasha et al., 2009; Landois et al., 2009). Accordingly, the present study sought to investigate the effect of the addition of group VI metals (Cr, Mo, and W) to the Ni/MgO catalyst on the yield and morphology of as-grown CNTs.

Experimental

The monometallic 5%Ni/MgO and the bimetallic 4%Ni-1%Cr/MgO, 4%Ni-1%Mo/MgO, and 4%Ni-1%W/MgO catalysts were prepared by impregnation and co-impregnation, respectively. Typically, the desired quantities of the metal precursors, $Ni(NO_3)_2 \cdot 6H_2O$, $(NH_4)_2CrO_4$, $(NH_4)_6Mo_7O_{24} \cdot 4H_2O$, and $(NH_4)_{10}(W_{12}O_{41}) \cdot 5H_2O$ salts (all analytical reagent grades, Sigma–Aldrich) were dissolved in sufficient quantities of deionised water then added to the required amount of calcined MgO support. Subsequently, the solutions were stirred at ambient temperature for 1 h, followed by sonication for 10 min to obtain homogenous mixtures. Finally, these mixtures were dried at 120 ℃ for 12 h prior to calcination in air at 600 ℃ for 4 h.

The process of growing CNTs operated using a fixed-bed horizontal-flow quartz reactor (100 cm in length and 3 cm in diameter). Typically, approximately 0.5 g of freshly calcined catalyst was dispersed in a porcelain boat and placed in the middle of the reactor. The temperature was increased to 500 ℃ under an argon (99.996 %) flow of 400 cm^3 min^{-1} (under standard conditions), then a hydrogen (99.9990 %) flow of 100 cm^3 min^{-1} was introduced at this temperature for 60 min to reduce the catalyst. The furnace was heated to the growth temperature of 850 ℃ under argon flow. After equilibration, a fed mixture of ethylene (99.90 %) at 100 cm^3 min^{-1} and 400 cm^3 min^{-1} of argon was introduced for 30 min. Finally, the system was cooled to ambient temperature under an argon flow of 100 cm^3 min^{-1}. The flow of the gases was controlled using the respective digital mass-flow controllers.

Powder X-ray diffraction experiments were performed on the fresh and used catalysts using X'Pert PRO MPD PANalytical (Almelo, The Netherlands). The patterns were recorded using CuK_α radiation ($\lambda = 0.1541$ nm) and a 2θ range from 10° to 90°.

The fresh catalysts were characterised by N_2 adsorption/desorption isotherms obtained at the temperature of liquid nitrogen in an automated physisorption instrument (Autosorb-1C, Quantachrome Instruments, Boynton Beach, FL, USA). Prior to the measurement, the catalysts were outgassed in vacuum at 200 ℃ for 2 h. The specific surface areas were calculated in accordance with the Brunauer–Emmett–Teller (BET) method.

The morphology of as-grown CNTs was investigated by transmission electron microscopy (TEM, Model JEM-200CX, JEOL, Tokyo, Japan). A small quantity of the catalyst plus the carbon deposit mixture was dispersed in 10 cm^3 of ethanol and sonicated for 10 min. A few drops of the resulting suspension were placed on a covered copper grid.

Thermogravimetric analysis was performed using an SDT; Q600 apparatus using 20 mg of catalysts at a heating rate of 10 ℃ min^{-1} in an air flow of 50 cm^3 min^{-1}. The carbon yield for each catalyst was calculated using the following equation:

$$\text{Carbon yield (\%)} = (\text{\% mass loss by carbon oxidation/\% of residue after oxidation}) \times 100 \quad (1)$$

Scanning electron micrographs were taken using a JSM-5300 microscope (JEOL, Tokyo, Japan). The samples were coated with Au for 5 min prior to the test.

The Raman spectra of the as-grown carbon nanotube samples were achieved at ambient temperature using a SENTERRA Dispersive Raman Microscope (Bruker, Ettlingen, Germany) equipped with a diode Nd:YAG laser and a wavelength of 532 nm from 500 cm^{-1} to 2000 cm^{-1}.

Results and discussion

The XRD patterns of the fresh catalysts after calcination at 600 ℃ for 4 h are depicted in Fig. 1. The catalysts are crystalline, as is evident from the sharpness of all the diffraction peaks. Moreover, the XRD spectra of all the catalysts exhibit the crystallite peaks at $2\theta = 37.2°$, 43.2°, and 62.7° which are characteristic of the formation of a rock-salt $Mg_xNi_{(1-x)}O$ solid

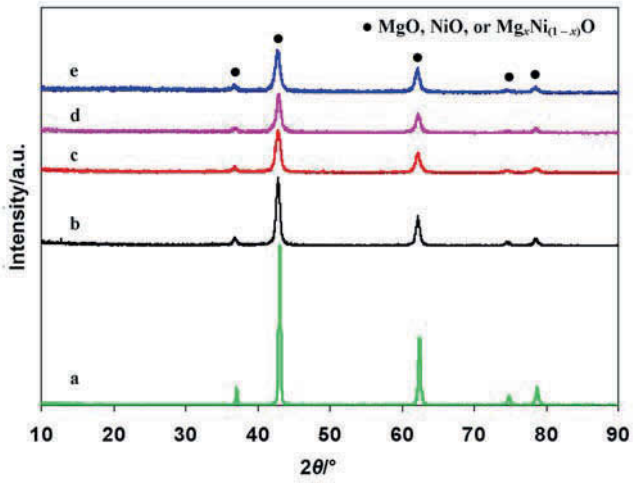

Fig. 1. XRD patterns of fresh calcined catalysts MgO (a), 5%Ni/MgO (b), 4%Ni-1%Cr/MgO (c), 4%Ni-1%Mo/MgO (d), and 4%Ni-1%W/MgO (e).

solution (Fig. 1). It is known that the NiO and MgO components in the catalyst exhibit similar diffraction planes (Figs. 1a and b), because the Ni^{2+} and Mg^{2+} ions have similar valence, ionic radius values [$r(Ni^{2+})$ = 0.07 nm and $r(Mg^{2+})$ = 0.065 nm], and crystal cell dimensions. Hence, the NiO and MgO components in the catalyst can readily form an $Mg_xNi_{(1-x)}O$ solid solution due to the excellent mutual solubility (Chen et al., 2006; Pour et al., 2005; Song & Pan, 2004), as shown in Fig. 1. The formation of the $Mg_xNi_{(1-x)}O$ solid solution is principally due to the interaction between the MgONi alloy with the exposed air atmosphere during the calcination step.

Furthermore, it is noted that the intensity of all the diffraction peaks, especially the principal MgO peak at 2θ = 42.8°, is significantly decreased by the addition of 1 mass % of group VI (Cr, Mo, or W) metals to 4%Ni/MgO catalyst in accordance with the following order: 5 Ni/MgO, 4%Ni-1%Cr/MgO, 4%Ni-1%Mo/MgO, 4%Ni-1%W/MgO. It may be assumed that the diffraction intensities decrease with increasing the atomic mass of group VI metals. This behaviour suggests that the addition of these metals induces a stronger interaction with the structural MgO and NiO crystals; this is reflected in the decrease in the MgO portion. In addition, none of the characteristic peaks of any known crystalline phases of the metal oxides or the $MgCr_2O_4$, $MgMoO_4$ as well as $MgWO_4$ species are observed in the XRD patterns of the fresh catalysts. Also, the Ni–(Cr, Mo, and W) species, i.e. $NiCr_2O_4$, $NiMoO_4$, and $NiWO_4$ are not detected in the XRD patterns (Fig. 1). This may indicate that the metal particles are well dispersed on the support and that the observed diffraction peaks are characteristic of only the MgO solid support.

It is important to note that the lower intensity of the diffraction peaks in the XRD patterns of the Ni–Mo/MgO and Ni–W/MgO catalysts indicates that the metal–support interaction between the bimetallic Ni–Mo or Ni–W combination with the MgO lattice greatly exceeds those between the monometallic Ni or bimetallic Ni–Cr and the MgO. This observation also reveals that the addition of group VI metals enhances the dispersion of Ni particles on the MgO solid support. Accordingly, it may be assumed that the Ni–Mo/MgO or Ni–W/MgO catalysts acquire a higher metal dispersion than the monometallic Ni/MgO or bimetallic Ni–Cr/MgO catalysts. This may be deemed to be one of the most important factors influencing the catalytic growth activity of the catalysts.

The thermogravimetric analysis was performed to evaluate the thermal properties of the as-produced CNTs. The mass loss is attributed mainly to the burn-

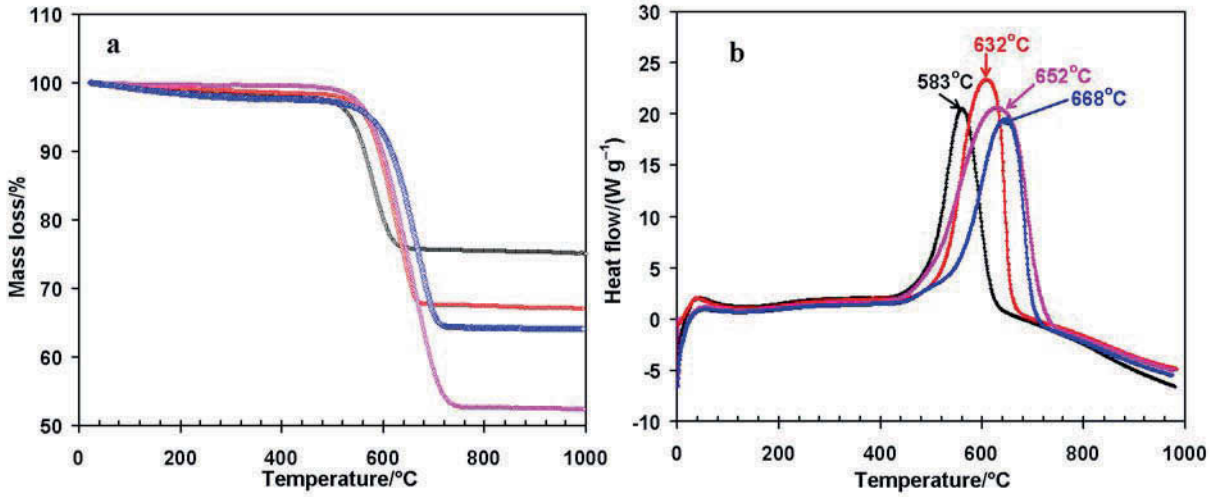

Fig. 2. Thermogravimetric (a) and differential thermal (b) analysis of as-grown CNTs over 5%Ni/MgO (black curve), 4%Ni-1%Cr/MgO (red curve), 4%Ni-1%Mo/MgO (pink curve), and 4%Ni-1%W/MgO (blue curve) catalysts.

Table 1. TGA data of as-grown CNTs over catalysts used

Catalysts	Temperature/ ℃			Carbon yield
	onset	end	inflection	mass %
5%Ni/MgO	501	627	583	28.6
4%Ni-1%Cr/MgO	509	667	632	44.3
4%Ni-1%Mo/MgO	512	741	652	87.4
4%Ni-1%W/MgO	525	718	668	50.9

ing of the deposited carbon in oxygen, hence it corresponds to the carbon yield in the catalysts. Accordingly, the oxidative stability curves of the CNTs over the catalysts are shown in Fig. 2. It may be observed that all the catalysts display a similar oxidation trend with a one-step degradation (Fig. 2a). This is indicative of the absence of amorphous carbon, hence high purity CNTs are obtained. It has been reported that the oxidation temperature of amorphous carbon is in the range of 200–400 ℃ (Yoshida et al., 2006). From the data shown in Fig. 2a, the calculated carbon yield is presented in Table 1. It is clear that the highest yield of CNTs (87.4 %) was achieved over the Ni–Mo/MgO catalyst, whereas the unprompted Ni/MgO catalyst exhibited the lowest carbon yield (28.6 %). Moreover, the onset temperature was almost equal for all catalysts, whereas the end-temperature was somewhat higher for Ni–Mo/MgO and Ni–W/MgO catalysts. In addition, the inflection temperature (oxidation temperature) of CNT was significantly higher over the later catalysts (741 ℃ and 718 ℃, respectively). This indicates that the as-produced CNTs over Ni–Mo/MgO or Ni–W/MgO acquired a higher thermal stability and quality than the other catalysts. In general, the TGA results showed that the incorporation of group VI metals enhanced the catalytic growth activity of the Ni/MgO catalyst. Hence, the activity of the catalysts in terms of CNT yield and quality can be arranged in the following order: Ni–Mo/MgO, Ni–W/MgO, Ni–Cr/MgO, Ni.

A comparison of the XRD patterns from the four catalysts after the reaction and without purification shows the appearance of the graphite peak at 2θ = 25.5° assigned to the graphitic carbon of MWCNTs. The relative intensity of this peak is higher for both the Ni–Mo/MgO and Ni–W/MgO catalysts than for Ni/MgO and Ni–Cr/MgO catalysts (Fig. 3). It may be stated that the intensity of the graphite peak and, consequently, the catalytic activities increase gradually with increasing the atomic mass of group VI metals up to Mo metal, beyond which the activity decreases slightly when using W as a promoter (Fig. 3). The data are in good agreement with the TGA results (Fig. 2 and Table 1).

Table 2 displays the XRD data for graphitic carbon over the catalysts. It is observed that the interlayer d-

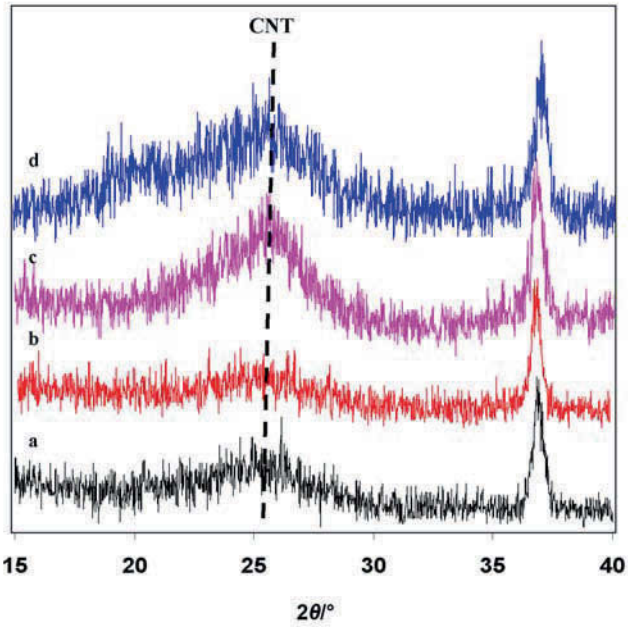

Fig. 3. XRD patterns of deposited carbon over 5%Ni/MgO (a), 4%Ni-1%Cr/MgO (b), 4%Ni-1%Mo/MgO (c), and 4%Ni-1%W/MgO (d) catalysts.

Table 2. XRD data of catalysts used

Catalyst	2θ/°	FWHM	d-spacing/nm
5% Ni/Al_2O_3	25.89	0.2245	0.32443
4%Ni-1%Cr/Al_2O_3	25.77	0.0900	0.32774
4%Ni-1%Mo/Al_2O_3	25.59	0.1569	0.33671
4%Ni-1% W/Al_2O_3	25.83	0.2176	0.34223

spacing values of graphite (002) at approximately 2θ = 25° over both the Ni–Mo/MgO and Ni–W/MgO catalysts (0.3367 nm and 0.3342 nm, respectively) are very close to the value of an ideal graphite crystal (0.3354 nm). This indicates that the addition of Mo or W metals to Ni/MgO enhances the degree of graphitisation and the crystallinity of the as-produced carbon nanotubes.

The higher catalytic growth activity of carbon nanotubes over the Ni–Mo/MgO catalyst can be attributed to the improvement in the stability and dispersion of Ni particles upon the addition of Mo metal. The enhancement in metal dispersion arises from the interaction between nickel oxide and molybdenum oxide to form a nickel molybdate species ($NiMoO_4$). Several studies have reported that the addition of molybdenum leads to a synergistic effect with Co (Tang et al., 2001; Flahaut et al., 2004; Kitiyanan et al., 2000). Tungsten could play a similar role (Willems et al., 2002). Additionally, molybdenum can be considered as the most effective centre for enhancing the aro-

matisation of methane under non-oxidative conditions (Wang et al., 1993; Aboul-Gheit et al., 2011, 2012). At the initial stage of the reaction, MoO_3 can be easily transformed to Mo_2C species (Aboul-Gheit et al., 2008; Aboul-Gheit & Awadallah, 2009). The molybdenum carbide species could provide the active centres continuously i.e. Ni metal particles by carbon during the nucleation step (Zhou et al., 2005). Zhou et al. (2006) stated that the Mo carbide played an important role in the synthesis of thin CNTs bundles, in which Mo_2C acted as a carbon reservoir.

The surface area affords a further explanation for the higher catalytic growth activities after incorporating group VI metals into Ni/MgO catalyst. Table 3 presents the surface area and crystallite size of the current catalysts under investigation. It is evident that the addition of group VI metals induces a significant increase in surface area. The Ni–Mo/MgO catalyst exhibits the highest surface area of 124 $m^2\ g^{-1}$, whereas the surface area for the monometallic Ni/MgO catalyst is only 76 $m^2\ g^{-1}$ (Table 3). The data in Table 3 indicate that the surface area increases with increasing the crystallite size of the catalysts in the case of bimetallic catalysts. This behaviour reveals that the incorporation of group VI metals could generate a mesoporous structure. The mesoporous structure may be attributed to the formation of $MgCr_2O_4$, $MgMoO_4$, or $MgWO_4$ spinel structures as a result of the interaction between group VI metals and the MgO support.

Table 3. Surface area and crystallite size of fresh calcined catalysts

Catalyst	Specific surface area	Crystallite size
	$m^2\ g^{-1}$	nm
5 Ni/Al_2O_3	76	3.44
4%Ni-1%Cr/Al_2O_3	103	1.89
4%Ni-1%Mo/Al_2O_3	124	2.91
4%Ni-1%W/Al_2O_3	116	3.15

In addition, the characterisation of fresh catalysts by XRD did not afford particle size determination

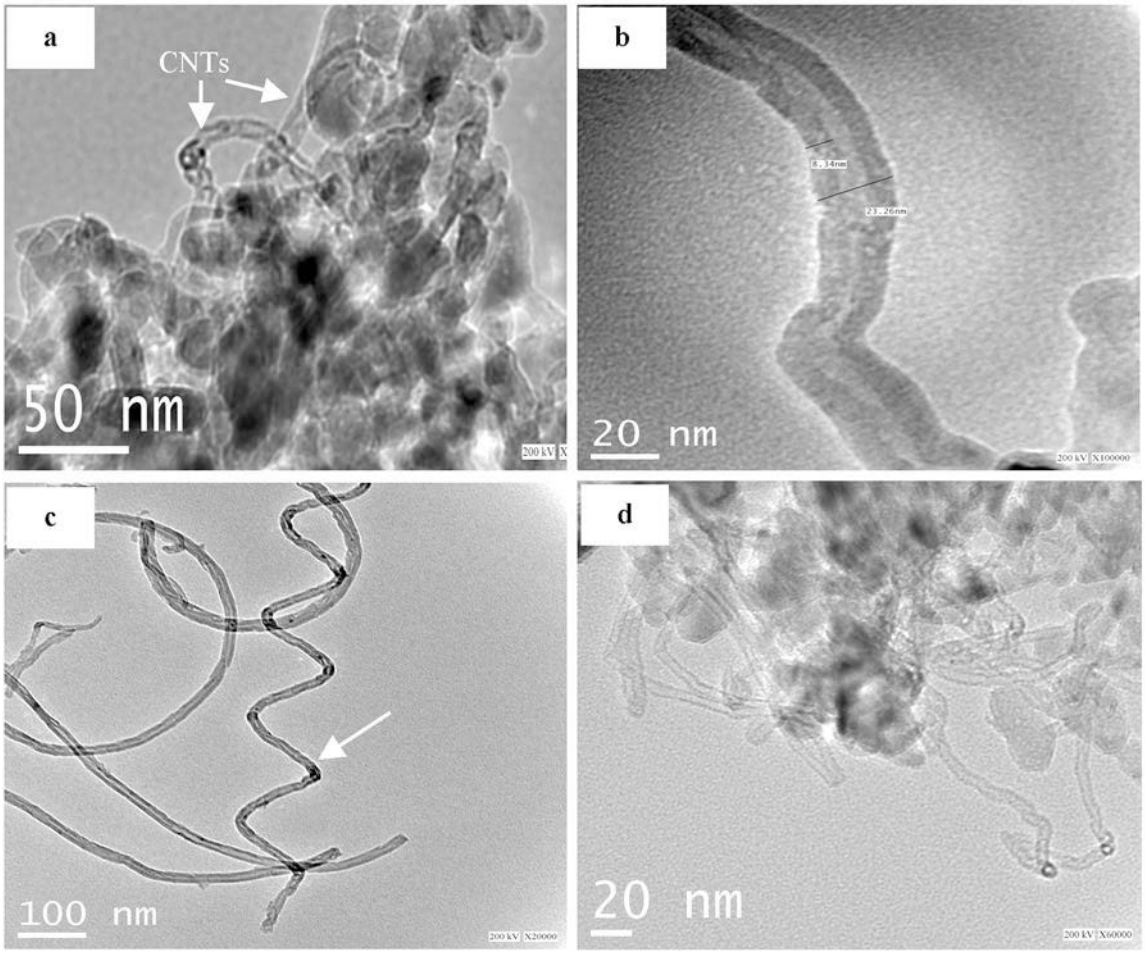

Fig. 4. TEM images of deposited carbon on 5%Ni/MgO (a), 4%Ni-1%Cr/MgO (b), 4%Ni-1%Mo/MgO (c), and 4%Ni-1%W/MgO (d) catalysts.

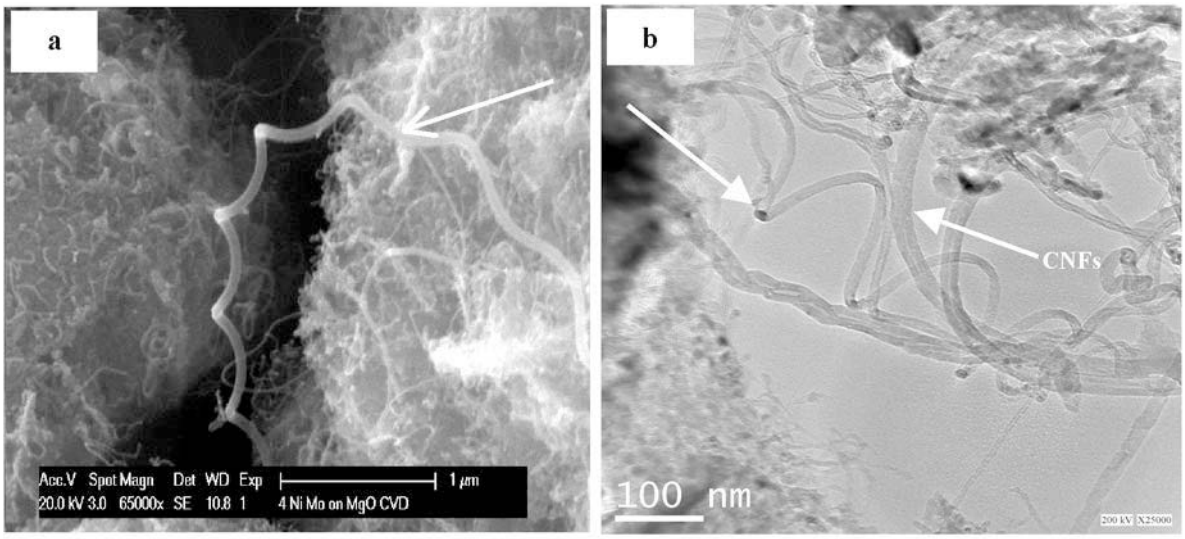

Fig. 5. SEM (a) and TEM (b) images of MWCNTs produced on 4%Ni-1%Mo/MgO catalyst.

of NiO due to formation of the $Mg_xNi_{(1-x)}O$ solid solution, but we can calculate the crystallite size of the catalysts using the well-known Scherrer equation (Table 3). The crystallite sizes of the catalysts were calculated from the main diffraction peak at $2\theta = 43.2°$ which corresponded to the $Mg_xNi_{(1-x)}O$ phase (Fig. 1). Hence, the crystallite sizes of the catalysts are greatly reduced upon addition of the group VI metals. These features demonstrate that the inclusion of Cr, Mo, and W metals in the structure of the Ni/MgO catalyst improves the dispersion and stabilisation of Ni particles on the catalysts.

The inhibition of the catalytic growth activity of the monometallic 5%Ni/MgO is largely attributed to the formation of the rock-salt $Mg_xNi_{(1-x)}O$ solid solution as is demonstrated by the XRD patterns (Fig. 1). The formation of the $Mg_xNi_{(1-x)}O$ solid solution reduces the extraction of Ni-active sites which are available for ethylene decomposition due to the strong metal support interaction. It is known that the metal–support interaction (MSI) could influence the reduction of metal oxide as well as the metal dispersion on supported catalysts. A strong MSI increases the difficulty associated with reduction of the metal oxide via increasing the reduction temperature or the formation of metal–support species ($Mg_xNi_{(1-x)}O$) which is difficult to reduce (Tauster et al., 1981, Tauster, 1987). In addition, a strong MSI decreases the aggregation of metal particles on the support surface leading to an enhancement in the metal dispersion. A strong MSI often leads to a low carbon yield and a short life-time for the catalyst, which may be due to the difficulty in detaching the metal particles from the support (Li et al., 2011).

Fig. 4 shows the TEM images of the as-produced CNTs on the catalysts. It is clear that the morphology has a tubular structure, reflecting the formation of MWCNTs with clear boundaries between the tubes. The unprompted Ni/MgO produced a rather low quantity of CNTs on its surface, indicating the low ability of this catalyst to grow filamentous carbon. The catalyst particles predominate over the number of CNTs (Fig. 4a). Moreover, the amorphous carbon may be formed in addition to the CNT, as shown in Fig. 4a. The TEM image of the as-grown CNTs over the Ni–Cr/MgO catalyst presents good graphitisation structures where the defects in the outer walls are not observed (Fig. 4b). Carbon nanotubes with helical, straight, and ring-shapes are obtained on the Ni–Mo/MgO catalyst (Fig. 4c). The SEM and TEM pictures (Fig. 5) confirm that the Ni–Mo/MgO catalyst produces a spiral-shaped carbon nanotube. Beside the CNTs' formation on the Ni–Mo/MgO catalyst, some carbon nanofibres (CNFs) were also detected, as shown in Fig. 5b. In addition, the length of the CNTs grown over the Ni–Mo/MgO catalyst is longer than the other catalysts, confirming the higher catalytic efficiency.

On the other hand, the CNTs were grown in a high density on the Ni–W/MgO catalyst. The CNT diameters appeared to have uniform diameters, indicating a good distribution of nickel particles in the catalyst due to the incorporation of W (Fig. 4d). This also demonstrates that the W could further protect the Ni particles from aggregation, leading to a smaller as well as a controlled particle size. Herrera and Resasco (2003) reported that the selectivity of the W/Co catalysts toward SWCNT depended on the stabilisation of the Co^{2+} ions, which resulted from an interaction with tungsten.

The degree of graphitisation and crystallinity of the as-synthesised MWCNTs on the catalysts were also investigated by Raman spectroscopy, as depicted in Fig. 6. Each spectrum displays a strong vibration near 1585 cm^{-1} (G band) due to the inter-plane sp^2

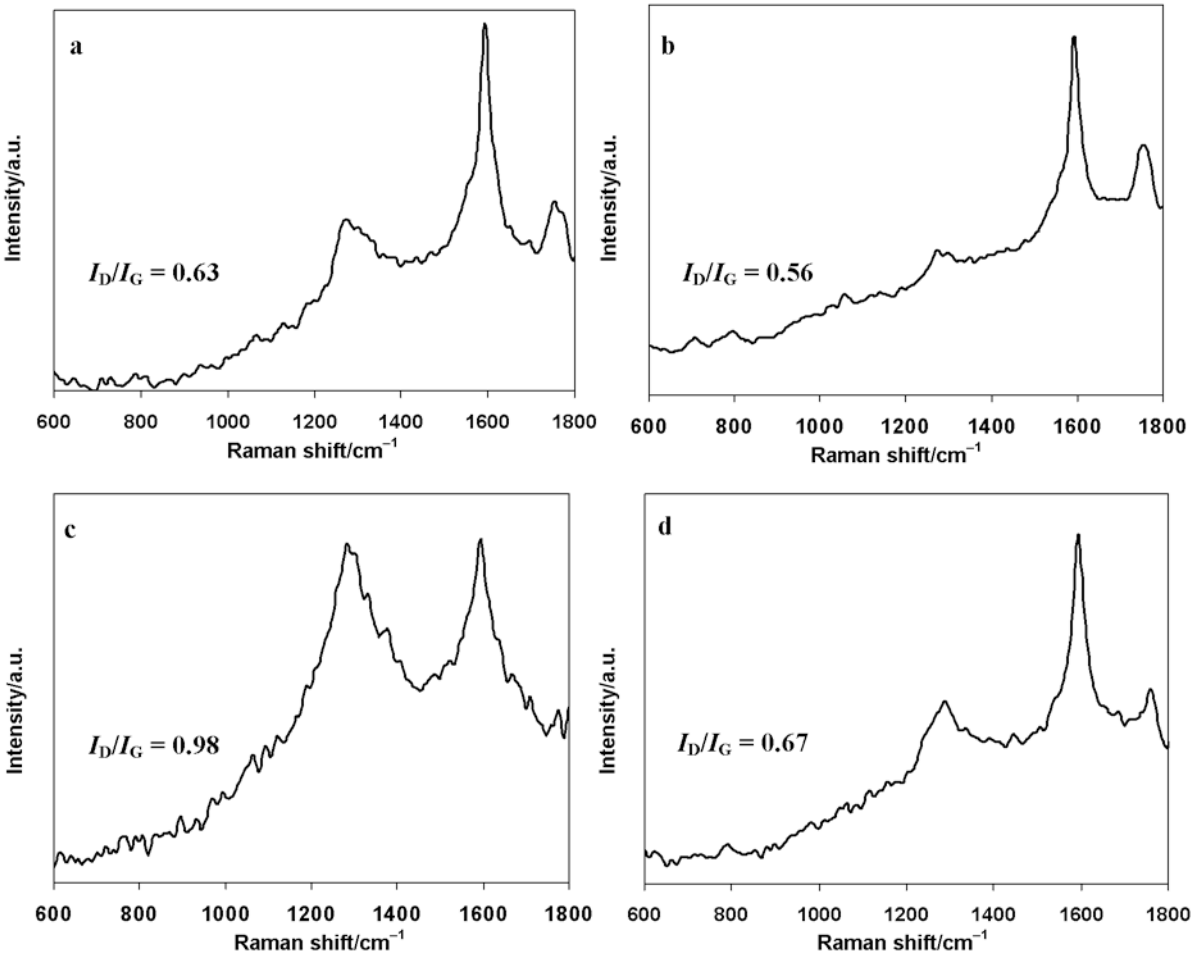

Fig. 6. Raman spectra of as-produced MWCNTs on 5%Ni/MgO (a), 4%Ni-1%Cr/MgO (b), 4%Ni-1%Mo/MgO (c), and 4%Ni-1%W/MgO (d) catalysts.

C—C-stretching, assigned to the characteristic feature of a graphitised tube. Another band appeared at 1330 cm^{-1} denoted as the D band, arising from the existence of disordered graphitised carbon due to defects, impurities, and presence of amorphous carbon on the sidewall of CNTs (Dresselhaus et al., 2002). The appearance of the D band is a clear indicator of the formation of MWCNTs. The D band in the samples under investigation arises from the structural disorder in the tube and not from the presence of amorphous carbon. This result is in good agreement with the TGA data (Fig. 2). In addition, the I_D/I_G ratio is regarded as an important parameter for investigating the quality and crystallinity of the CNTs. The lower ratio of (I_D/I_G) indicates that the CNT acquires a higher degree of crystallisation and graphitisation. As shown in Fig. 6, the ratios of I_D/I_G for all the deposited carbon nanomaterial on the catalysts are lower than unity (0.56–0.98), indicating that the as-grown CNTs have good crystallinity of graphite sheets as well as fewer defects and impurities.

Conclusions

Multi-walled carbon nanotubes (MWCNTs) were successfully prepared by using monometallic Ni/MgO and bimetallic Ni–M (M = Cr, Mo, and W)/MgO catalysts. The addition of group VI metals (1 mass %) induced a significant improvement in the catalytic growth activity for the synthesis of CNT by the decomposition of C_2H_4. It was shown that increasing the atomic mass of group VI metals up to Mo leads to a progressive enhancement in the yield of MWCNTs. Surface area and metal dispersion were improved subsequent to the incorporation of these metals. The formation of an $Mg_xNi_{(1-x)}O$ solid solution was the main reason for the lower catalytic growth activity of monometallic Ni/MgO catalyst. The addition of a group VI metal causes a strong interaction with NiO which inhibits the formation of a solid solution, leading to an increase in catalytic performance The TEM, XRD, and TGA results revealed that the as-grown CNTs on the Ni–Mo/MgO catalyst achieved a higher degree of crystallinity and graphitisation than with

the other catalysts. The CNTs synthesised using the Ni–W/MgO catalyst have a more uniform diameter and higher quality, indicating good dispersion of the Ni particles.

References

Aboul-Gheit, A. K., Awadallah, A. E., El-Kossy, S. M., & Mahmoud, A. L. H. (2008). Effect of Pd or Ir on the catalytic performance of Mo/H-ZSM-5 during the non-oxidative conversion of natural gas to petrochemicals. *Journal of Natural Gas Chemistry*, *17*, 337–343. DOI: 10.1016/s1003-9953(09)60005-0.

Aboul-Gheit, A. K., & Awadallah, A. E. (2009). Effect of combining the metals of group VI supported on H-ZSM-5 zeolite as catalysts for non-oxidative conversion of natural gas to petrochemicals. *Journal of Natural Gas Chemistry*, *18*, 71–77. DOI: 10.1016/s1003-9953(08)60080-8.

Aboul-Gheit, A. K., Awadallah, A. E., Aboul-Enein, A. A., & Mahmoud, A. L. H. (2011). Molybdenum substitution by copper or zinc in H-ZSM-5 zeolite for catalyzing the direct conversion of natural gas to petrochemicals under non-oxidative conditions. *Fuel*, *90*, 3040–3046. DOI: 10.1016/j.fuel.2011.05.010.

Aboul-Gheit, A. K., El-Masry, M. S., & Awadallah, A. E. (2012). Oxygen free conversion of natural gas to useful hydrocarbons and hydrogen over monometallic Mo and bimetallic Mo–Fe, Mo–Co or Mo–Ni/HZSM-5 catalysts prepared by mechanical mixing. *Fuel Processing Technology*, *102*, 24–29. DOI: 10.1016/j.fuproc.2012.04.017.

Ago, H., Uehara, N., Yoshihara, N., Tsuji, M., Yumura, M., Tomonaga, N., & Setoguchi, T. (2006). Gas analysis of the CVD process for high yield growth of carbon nanotubes over metal-supported catalysts. *Carbon*, *44*, 2912–2918. DOI: 10.1016/j.carbon.2006.05.049.

Andersen, S. M., Borghei, M., Lund, P., Elina, Y. R., Pasanen, A., Kauppinen, E., Ruiz, V., Kauranen, P., & Skou, E. M. (2013). Durability of carbon nanofiber (CNF) & carbon nanotube (CNT) as catalyst support for Proton Exchange Membrane Fuel Cells. *Solid State Ionics*, *231*, 94–101. DOI: 10.1016/j.ssi.2012.11.020.

Ashok, J., Kumar, S. N., Venugopal, A., Kumari, V. D., & Subrahmanyam, M. (2007). CO_x-free H_2 production via catalytic decomposition of CH_4 over Ni supported on zeolite catalysts. *Journal of Power Sources*, *164*, 809–814. DOI: 10.1016/j.jpowsour.2006.11.029.

Awadallah, A. E., Aboul-Enein, A. A., & Aboul-Gheit, A. K. (2014). Effect of progressive Co loading on commercial Co–Mo/Al_2O_3 catalyst for natural gas decomposition to CO_x-free hydrogen production and carbon nanotubes. *Energy Conversion and Management*, *77*, 143–151. DOI: 10.1016/j.enconman.2013.09.017.

Cassell, A. M., Raymakers, J. A., Kong, J., & Dai, H. J. (1999). Large scale CVD synthesis of single-walled carbon nanotubes. *The Journal of Physical Chemistry B*, *103*, 6484–6492. DOI: 10.1021/jp990957s.

Chai, S. P., Zein, S. H. S., & Mohamed, A. R. (2006). Preparation of carbon nanotubes over cobalt-containing catalysts via catalytic decomposition of methane. *Chemical Physics Letter*, *426*, 345–350. DOI: 10.1016/j.cplett.2006.05.026.

Chen, M. H., Huang, Z. C., Wu, G. T., Zhu, G. M., You, J. K., & Lin, Z. G. (2003). Synthesis and characterization of SnO–carbon nanotube composite as anode material for lithium-ion batteries. *Materials Research Bulletin*, *38*, 831–836. DOI: 10.1016/s0025-5408(03)00063-1.

Chen, C. M., Dai, Y. M., Huang, J. G., & Jehng, J. M. (2006). Intermetallic catalyst for carbon nanotubes (CNTs) growth by thermal chemical vapor deposition method. *Carbon*, *44*, 1808–1820. DOI: 10.1016/j.carbon.2005.12.043.

Chen, L., Liu, H. T., Yang, K., Wang, J. K., & Wang, X. L. (2009). Catalytic synthesis of carbon nanotubes from the decomposition of methane over a Ni–Co/La_2O_3 catalyst. *Canadian Journal of Chemistry*, *87*, 47–53. DOI: 10.1139/v08-077.

de Lucas, A., Garrido, A., Sánchez, P., Romero, A., & Valverde, J. L. (2005). Growth of carbon nanofibers from Ni/Y zeolite based catalysts: Effects of Ni introduction method, reaction temperature, and reaction gas composition. *Industrial & Engineering Chemistry Research*, *44*, 8225–8236. DOI: 10.1021/ie058027k.

Dresselhaus, M. S., Dresselhaus, G., Jorio, A., Souza Filho, A. G., & Saito, R. (2002). Raman spectroscopy on isolated single wall carbon nanotubes. *Carbon*, *40*, 2043–2061. DOI: 10.1016/s0008-6223(02)00066-0.

Dupuis, A. C. (2005). The catalyst in the CCVD of carbon nanotubes—a review. *Progress in Materials Science*, *50*, 929–961. DOI: 10.1016/j.pmatsci.2005.04.003.

Fan, S. S., Chapline, M. G., Franklin, N. R., Tombler, T. W., Cassell, A. M., & Dai, H. J. (1999). Self-oriented regular arrays of carbon nanotubes and their field emission properties. *Science*, *283*, 512–514. DOI: 10.1126/science.283.5401.512.

Flahaut, E., Peigney, A., Bacsa, W. S., Bacsa, R. R., & Laurent. Ch. (2004). CCVD synthesis of carbon nanotubes from (Mh,Co,Mo)O catalysts: influence of the proportions of cobalt and molybdenum. *Journal of Materials Chemistry*, *14*, 646–653. DOI: 10.1039/b312367g.

Fujiwara, A., Ishii, K., Suematsu, H., Kataura, H., Maniwa, Y., Suzuki, S., & Achiba, Y. (2001). Gas adsorption in the inside and outside of single-walled carbon nanotubes. *Chemical Physics Letter*, *336*, 205–211. DOI: 10.1016/s0009-2614(01)00111-7.

Harutyunyan, A. R., Pradhan, B. K., Kim, U. J., Chen, G. G., & Eklund, P. C. (2002). CVD synthesis of single wall carbon nanotubes under "soft" conditions. *Nano Letters*, *2*, 525–530. DOI: 10.1021/nl0255101.

Herrera, J. E., & Resasco, D. E. (2003). Role of Co–W interaction in the selective growth of single-walled carbon nanotubes from CO disproportionation. *The Journal of Physical Chemistry B*, *107*, 3738–3746. DOI: 10.1021/jp027602k.

Jehng, J. M., Tung, W. C., & Kuo, C. H. (2008). The formation mechanisms of multi-wall carbon nanotubes over the Ni modified MCM-41 catalysts. *Journal of Porous Materials*, *15*, 43–51. DOI: 10.1007/s10934-006-9050-x.

Kitiyanan, B., Alvarez, W. E., Harwell, J. H., & Resasco, D. E. (2000). Controlled production of single-wall carbon nanotubes by catalytic decomposition of CO on bimetallic Co–Mo catalysts. *Chemical Physics Letter*, *317*, 497–503. DOI: 10.1016/s0009-2614(99)01379-2.

Landois, P., Peigney, A., Laurent, Ch., Frin, L., Datas, L., & Flahaut, E. (2009). CCVD synthesis of carbon nanotubes with W/Co–MgO catalysts. *Carbon*, *47*, 789–794. DOI: 10.1016/j.carbon.2008.11.018.

Lee, C. J., Park, J. H., Kim, J. M., Huh, Y., Lee, J. Y., & No, K. S. (2000). Low-temperature growth of carbon nanotubes by thermal chemical vapor deposition using Pd, Cr, and Pt as co-catalyst. *Chemical Physics Letter*, *327*, 277–283. DOI: 10.1016/s0009-2614(00)00877-0.

Li, Y., Zhang, B. C., Tang, X. L., Xu, Y. D., & Shen, W. J. (2006). Hydrogen production from methane decomposition over Ni/CeO_2 catalysts. *Catalysis Communications*, *7*, 380–386. DOI: 10.1016/j.catcom.2005.12.002.

Li, Y. D., Li, D. X., & Wang, G. W. (2011). Methane decomposition to CO_x-free hydrogen and nano-carbon material on group 8–10 base metal catalysts: A review. *Catalysis Today*, *162*, 1–48. DOI: 10.1016/j.cattod.2010.12.042.

Loebick, C. Z., Derrouiche, S., Fang, F., Li, N., Haller, G. L., & Pfefferle, L. D. (2009). Effect of chromium addition to the Co-MCM-41 catalyst in the synthesis of single wall carbon nanotubes. *Applied Catalysis A: General*, *368*, 40–49. DOI: 10.1016/j.apcata.2009.08.004.

Loebick, C. Z., Lee, S. C., Derrouiche, S., Schwab, M., Chen, Y., Haller, G. L., & Pfefferle, L. (2010). A novel synthesis route for bimetallic CoCr–MCM-41 catalysts with higher metal loadings. Their application in the high yield, selective synthesis of Single-Wall Carbon Nanotubes. *Journal of Catalysis*, *271*, 358–369. DOI: 10.1016/j.jcat.2010.02.021.

Ni, L., Kuroda, K., Zhou, L. P., Kizuka, T., Ohta, K., Matsuishi, K., & Nakamura, J. (2006). Kinetic study of carbon nanotube synthesis over Mo/Co/MgO catalysts. *Carbon*, *44*, 2265–2272. DOI: 10.1016/j.carbon.2006.02.031.

Pasha, M. A., Shafiekhani, A., & Vesaghi, M. A. (2009). Hot filament CVD of Fe–Cr catalyst for thermal CVD carbon nanotube growth from liquid petroleum gas. *Applied Surface Science*, *256*, 1365–1371. DOI: 10.1016/j.apsusc.2009.08.090.

Pour, A. N., Zamani Kheirolah, Y., Jozani, J., & Mehr, J. Y. (2005). The influence of La_2O_3 and TiO_2 on NiO/MgO/α-Al_2O_3. *Reaction Kinetics and Catalysis Letters*, *86*, 157–162. DOI: 10.1007/s11144-005-0307-1.

Sinnott, S. B., Andrews, R., Qian, D., Rao, A. M., Mao, Z., Dickey, E. C., & Derbyshire, F. (1999). Model of carbon nanotube growth through chemical vapor deposition. *Chemical Physics Letter*, *315*, 25–30. DOI: 10.1016/s0009-2614(99)01216-6.

Song, C. S., & Pan, W. (2004). Tri-reforming of methane: a novel concept for catalytic production of industrially useful synthesis gas with desired H_2/CO ratios. *Catalysis Today*, *98*, 463–484. DOI: 10.1016/j.cattod.2004.09.054.

Takenaka, S., Kobayashi, S., Ogihara, H., & Otsuka, K. (2003). Ni/SiO_2 catalyst effective for methane decomposition into hydrogen and carbon nanofiber. *Journal of Catalysis*, *217*, 79–87. DOI: 10.1016/s0021-9517(02)00185-9.

Tang, S., Zhong, Z., Xiong, Z., Sun, L., Liu, L., Lin, J., Shen, Z. X., & Tan, K. L. (2001). Controlled growth of single-walled carbon nanotubes by catalytic decomposition of CH_4 over Mo/Co/MgO catalysts. *Chemical Physics Letters*, *350*, 19–26. DOI: 10.1016/s0009-2614(01)01183-6.

Tans, S. J., Verschueren, A. R. M., & Dekker, C. (1998). Room-temperature transistor based on a single carbon nanotube. *Nature*, *393*, 49–52. DOI: 10.1038/29954.

Tauster, S. T., Fung, S. C., Baker, R. T. K., & Horsley, J. A. (1981). Strong interactions in supported-metal catalysts. *Science*, *211*, 1121–1125. DOI: 10.1126/science.211.4487.1121

Tauster, S. J. (1987). Strong metal–support interactions. *Accounts of Chemical Research*, *20*, 389–394. DOI: 10.1021/ar00143a001.

Toebes, M. L., Zhang, Y. H., Hájek, J., Nijhuis, T. A., Bitter, J. H., van Dillen, A. J., Murzin, D. Yu., Koningsberger, D. C., & de Jong, K. P. (2004). Support effects in the hydrogenation of cinnamaldehyde over carbon nanofiber-supported platinum catalysts: characterization and catalysis. *Journal of Catalysis*, *226*, 215–225. DOI: 10.1016/j.jcat.2004.05.026.

Wang, L. S., Tao, L. X., Xie, M. S., Xu, G. F., Huang, J. S., & Xu, Y. D. (1993). Dehydrogenation and aromatization of methane under non-oxidizing conditions. *Catalysis Letters*, *21*, 35–41. DOI: 10.1007/bf00767368.

Willems, I., Kónya, Z., Fonseca, A., & Nagy, J. B. (2002). Heterogeneous catalytic production and mechanical resistance of nanotubes prepared on magnesium oxide supported Co-based catalysts. *Applied Catalysis A: General*, *229*, 229–233. DOI: 10.1016/s0926-860x(02)00030-3.

Yeoh, W. M., Lee, K. Y., Chai, S. P., Lee, K. T., & Mohamed, A. R. (2010). The role of molybdenum in Co-Mo/MgO for large-scale production of high quality carbon nanotubes. *Journal of Alloys and Compounds*, *493*, 539–543. DOI: 10.1016/j.jallcom.2009.12.151.

Yoshida, A., Kaburagi, Y., & Hishiyama, Y. (2006). Full width at half maximum intensity of the G band in the first order Raman spectrum of carbon material as a parameter for graphitization. *Carbon*, *44*, 2333–2335. DOI: 10.1016/j.carbon.2006.05.020.

Zheng, G. B., Kouda, K., Sano, H., Uchiyama, Y., Shi, Y. F., & Quan, H. J. (2004). A model for the structure and growth of carbon nanofibers synthesized by the CVD method using nickel as a catalyst. *Carbon*, *42*, 635–640. DOI: 10.1016/j.carbon.2003.12.077.

Zhou, L. P., Ohta, K., Kuroda, K., Lei, N., Matsuishi, K., Gao, L. Z., Matsumoto, T., & Nakamura, J. (2005). Catalytic functions of Mo/Ni/MgO in the synthesis of thin carbon nanotubes. *The Journal of Physical Chemistry B*, *109*, 4439–4447. DOI: 10.1021/jp045284e.

Zhou, W. W., Han, Z. Y., Wang, J. Y., Zhang, Y., Jin, Z., Sun, X., Zhang, Y. W., Yan, C. H., & Li, Y. (2006). Copper catalyzing growth of single-walled carbon nanotubes on substrates. *Nano Letters*, *6*, 2987–2990. DOI: 10.1021/nl061871v.